Adduction of the Human *N-ras* Codon 61 Sequence with (−)-(7*S*,8*R*,9*R*,10*S*)-7,8-Dihydroxy-9,10-epoxy-7,8,9,10-tetrahydrobenzo[*a*]pyrene: Structural Refinement of the Intercalated SRSR(61,2) (−)-(7*S*,8*R*,9*S*,10*R*)-N^6-[10-(7,8,9,10-Tetrahydrobenzo[*a*]pyrenyl)]-2′-deoxyadenosyl Adduct from ^{1}H NMR†

Irene S. Zegar, Seong J. Kim,‡ Tommy N. Johansen,§ Pamela J. Horton, Constance M. Harris, Thomas M. Harris, and Michael P. Stone*

Center in Molecular Toxicology and Department of Chemistry, Vanderbilt University, Nashville, Tennessee 37235

Received October 17, 1995; Revised Manuscript Received January 18, 1996⊗

ABSTRACT: The structure of the (−)-(7*S*,8*R*,9*S*,10*R*)-N^6-[10-(7,8,910-tetrahydrobenzo[*a*]pyrenyl)]-2′-deoxyadenosyl adduct at X^6 of 5′-d(CGGACXAGAAG)-3′•5′-d(CTTCTTGTCCG)-3′, derived from *trans* addition of the exocyclic N^6-amino group of dA to (−)-(7*S*,8*R*,9*R*,10*S*)-7,8-dihydroxy-9,10-epoxy-7,8,9,10-tetrahydrobenzo[*a*]pyrene [(−)-DE2], was determined using molecular dynamics simulations restrained by 369 NOEs from ^{1}H NMR. This was named the SRSR(61,2) adduct, derived from the *N-ras* protooncogene at and adjacent to the nucleotides encoding amino acid 61 (underlined) of the p21 gene product. NOEs between C^5, $^{S,R,S,R}A^6$, and A^7 were disrupted, as were those between T^{17} and G^{18}. NOEs between benzo[*a*]pyrene and DNA protons were localized on the two faces of the pyrenyl ring. The benzo[*a*]pyrene H3−H6 protons showed NOEs to T^{17} CH_3, while H1, H2, and H3 showed NOEs to T^{17} deoxyribose; the latter protons and H4 showed NOEs to T^{17} H2′,H2″ and to T^{17} H6. NOEs were observed between H11 and H12 and C^5 H1′,H2′,H2″. G^{18} N1H showed NOEs to both faces of benzo[*a*]pyrene. Upfield shifts of 2.6 ppm for T^{17} N3H and 1.8 ppm for G^{18} N1H, 1 ppm for T^{17} H6 and CH_3, and 0.75 ppm for C^5 H5, with a smaller shift for C^5 H6, and a 1.5 ppm dispersion of the pyrenyl protons suggested that benzo[*a*]pyrene intercalated above the 5′-face of $^{S,R,S,R}A^6$. The precision of the refined structures was monitored by pairwise root mean square deviations, which were <1.5 Å; accuracy was measured by complete relaxation matrix calculations, which yielded a sixth root R factor of 8.1×10^{-2}. Interstrand stacking between the pyrenyl ring and the T^{17} pyrimidine and G^{18} purine rings was enhanced by the bay ring. Changes of +30° and −25° in buckle for C^5•G^{18} and $^{S,R,S,R}A^6$•T^{17}, respectively, were calculated, as was a −40° change in propeller twist for C^5•G^{18}. The rise between C^5•G^{18} and $^{S,R,S,R}A^6$•T^{17} was calculated to be 7 Å. The work extended the pattern for adenine N6 benzo[*a*]pyrene adducts, in which the *R* stereochemistry at C10 predicted 5′-intercalation of the pyrenyl moiety.

Interest in the polycyclic aromatic hydrocarbon (PAH)[1] class of chemical carcinogens dates to the Percival Pott observations in the 18th century, which linked the occurrence of scrotal cancer in chimney sweeps with occupational exposure to soot. The genotoxicity of PAH compounds is linked to metabolic activation into reactive electrophiles which react with DNA (Miller, 1970). In the case of benzo[*a*]pyrene, microsomal P_{450} enzymes [reviewed by Guengerich (1992)] catalyze formation of diastereomeric 7,8-dihydrodiol 9,10-epoxides (Sims et al., 1974), first synthesized by the Jerina (Yagi et al., 1975) and the Harvey (Beland & Harvey, 1976) laboratories. Benzo[*a*]pyrene is metabolized to produce bay-region epoxides, including (+)-(7*R*,8*S*,9*S*,10*R*)-7,8-dihydroxy-9,10-epoxy-7,8,9,10-tetrahydrobenzo[*a*]pyrene [(+)-DE2] and (−)-(7*S*,8*R*,9*R*,10*S*)-7,8-dihydroxy-9,10-epoxy-7,8,9,10-tetrahydrobenzo[*a*]pyrene [(−)-DE2].[2] Evidence that (+)-DE2 had the greatest bonding affinity to DNA was obtained from reactions using diastereomeric mixtures of the epoxides with DNA, followed by degradation and analysis (Weinstein et al., 1976; King et al., 1976). Identification of the DNA adducts (Jeffrey et al., 1977; Nakanishi et al., 1977) revealed an adduct formed between

† This research was supported by the NIH: ES-05355. Funding for the AMX-500 NMR spectrometer was supplied by the NIH shared instrumentation program, RR-05805, and the Vanderbilt Center in Molecular Toxicology, ES-00267.

* Author to whom correspondence should be addressed.

‡ Present address: Research and Development Center, Samsung Fine Chemicals, Co., Ltd., Yusong, Munjidong 103-1, Republic of South Korea.

§ Present address: Department of Medicinal Chemistry, The Royal Danish School of Pharmacy, Universitetsparken 2, DK-2100 Copenhagen, Denmark.

⊗ Abstract published in *Advance ACS Abstracts,* April 15, 1996.

[1] Abbreviations: BPDE, benzo[*a*]pyrenediol epoxide; DNA, deoxyribonucleic acid; DSS, sodium 4,4-dimethyl-4-silapentanesulfonate; EDTA, ethylenediaminetetraacetic acid; HPLC, high-pressure liquid chromatography; NMR, nuclear magnetic resonance; NOE, nuclear Overhauser enhancement; NOESY, two-dimensional NOE spectroscopy; ppm, parts per million; PAH, polycyclic aromatic hydrocarbon; PEM, potential energy minimization; rms, root mean square; TPPI, time-proportional phase increment; TOCSY, total homonuclear correlated spectroscopy; 1D, one dimensional; 2D, two dimensional.

[2] The empirical designations for these diol epoxides are the (±)-*anti*-BPDE, or (±)-DE2. Benzo[*a*]pyrene is also metabolized into two additional diol epoxides, (+)-(7*S*,8*R*,9*S*,10*R*)-7,8-dihydroxy-9,10-epoxy-7,8,9,10-tetrahydrobenzo[*a*]pyrene and (−)-(7*R*,8*S*,9*R*,10*S*)-7,8-dihydroxy-9,10-epoxy-7,8,9,10-tetrahydrobenzo[*a*]pyrene. These are the (±)-*syn*-BPDE, or (±)-DE1, which are generally regarded to be less mutagenic and tumorigenic.

S0006-2960(95)02473-1 CCC: $12.00

the 2-amino group of guanine and C10 of the PAH, and derived from (+)-DE2, to be the major product. Mutagenesis results were consistent with the hypothesis that the diastereomeric diol epoxides represented the ultimate carcinogenic species. (+)-DE2 was generally the most mutagenic form (Newbold & Brookes, 1976; Huberman et al., 1976). There has thus been considerable interest in the structures of benzo[*a*]pyrene (Cosman et al., 1992, 1993a, 1994a,b; De Los Santos et al., 1992; Fountain & Krugh, 1995) and related PAH (Cosman et al., 1995b) and styrene oxide (Zegar et al., 1996) adducts at guanine N2.

Minor products in the reaction of various diastereomeric BPDE with DNA have also been observed, including adenine N6 adducts (Jennette et al., 1977; Osborne et al., 1981). These are of interest since the extent to which prevalent adduction sites are related to prevalent mutagenic lesions remains unknown. Indeed, at lower and possibly physiologically relevant dosages, increased benzo[*a*]pyrene-induced mutagenesis at adenine was reported (Wei et al., 1991, 1993, 1994). Therefore, correlating the solution structures of benzo[*a*]pyrene and additional PAH adducts at adenines with mutations at adenines is an important goal. The structures of the (−)-(7*S*,8*R*,9*S*,10*R*)-*N*^{6}-[10-(7,8,9,10-tetrahydrobenzo[*a*]pyrenyl)]-2′-deoxyadenosyl and the (+)-(7*R*,8*S*,9*R*,10*S*)-*N*^{6}-[10-(7,8,9,10-tetrahydrobenzo[*a*]pyrenyl)]-2′-deoxyadenosyl adducts, each opposite dG in the complementary strand, were recently solved (Schurter et al., 1995b; Yeh et al., 1995), as was the structure of the (−)-7*R*,8*S*,9*R*,10*R*)-*N*^{6}-[10-(7,8,9,10-tetrahydrobenzo[*a*]pyrenyl)]-2′-deoxyadenosyl adduct opposite dT in the complementary strand (Schurter et al., 1995a). Structures for a diastereomeric pair of benzo[c]phenanthrene adducts opposite dT in the complementary strand were also reported (Cosman et al., 1993b, 1995a), and a series of diastereomeric and sequence isomeric styrene oxide adducts were reported by this laboratory (Feng et al., 1995, 1996).

The formation of adducts between DNA and metabolically activated chemical carcinogens, including the diastereomeric diol epoxides of benzo[*a*]pyrene, likely represents an early event in carcinogenesis (Miller, 1970, 1978). DNA adducts are generally believed to act by inducing somatic cell mutations, due to errors in replication or repair. Mutations in specific coding regions are correlated with carcinogenesis. Protooncogene coding sequences represent one set of genetic loci in which adduct-induced mutations might directly initiate cellular transformation. Mutations within a limited number of codons in the p21 gene, including codon 61, cause oncogene activation [reviewed by Barbacid (1987)]. Hence, it seems important to understand how DNA adducts of benzo[*a*]pyrene induce structural changes within the coding sequence at codon 61 of the *N-ras* gene.

Direct evidence that human tumors are induced by benzo[*a*]pyrene-induced mutations in codon 61 of the *N-ras* protooncogene is not available, but indirect evidence suggests adducts do induce mutations in and thereby activate protooncogenes such as *ras*. This evidence comes from comparison of mutations in carcinogen-induced tumors to known or suspected reaction sites of specific carcinogens [reviewed by Balmain and Brown (1988)], an example being the polycyclic aromatic hydrocarbon dimethylbenzanthracene (Quintanilla et al., 1986). In these studies it has been generally believed that the tumors were induced by specific chemical carcinogens to which the animals were exposed. Recently, it was reported that mammary tumors previously thought to have been induced by exposure to methylnitrosourea (MNU) (Zarbl et al., 1985) actually arose from cells having preexisting mutations in *H-ras* (Cha et al., 1994), thus leaving the question unanswered as to whether MNU directly activates *H-ras* via adduct-induced mutations in the protooncogene. The latter report notwithstanding, it continues to seem reasonable that DNA adducts located within critical coding regions of the *N-ras* protooncogene could induce activating mutations.

Chart 1: (A) SRSR(61,2) Oligodeoxynucleotide, Where X = (−)-(7*S*,8*R*,9*S*,10*R*)-*N*^{6}-[10-(7,8,9,10-Tetrahydrobenzo[*a*]-pyrenyl)]-2′-deoxyadenosyl Adduct (Bottom), and (B) the (−)-(7*S*,8*R*,9*S*,10*R*)-*N*^{6}-[10-(7,8,9-Trihydroxy-7,8,9,10-tetrahydrobenzo[*a*]pyrenyl)-2′-deoxyadenosyl Adduct and Designations of the Benzo[*a*]pyrene Protons

A

ras codons

60 61 62

5′-C^1 |G^2 G^3 A^4 |C^5 X^6 A^7 |G^8 A^9 A^{10}|G^{11}-3′

3′-G^{22}|$C^{21}C^{20}T^{19}$|$G^{18}T^{17}T^{16}$|$C^{15}T^{14}T^{13}$|C^{12}-5′

B

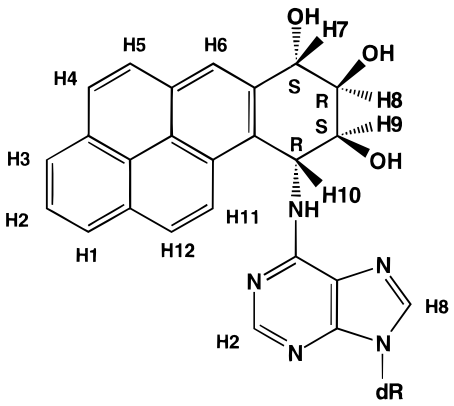

Structural refinement of the *ras61* oligodeoxynucleotide, d(CGGACAAGAAG)·d(CTTCTTGTCCG),[3] which contains the sequence for codons 60, 61 (underlined), and 62 of the human *N-ras* gene, was completed in this laboratory (Feng & Stone, 1995). A nonbiomimetic synthesis enabled large-scale production of site-specific (*R*)- and (*S*)-α-(*N*^{6}-adenyl)-styrene oxide-modified oligodeoxynucleotides, while simultaneously eliminating problems in controlling the regioselectivity of adduction (Harris et al., 1991). This chemistry was extended to production of the (−)-(7*S*,8*R*,9*S*,10*R*)-*N*^{6}-[10-(7,8,9,10-tetrahydrobenzo[*a*]pyrenyl)]-2′-deoxyadenosyl adduct (Kim et al., 1991, 1992; Harris et al., 1994), 5′-d(CGGACXAGAAG)-3′·5′-d(CTTCTTGTCCG)-3′, where X is the adducted adenine. This was named the SRSR(61,2) adduct, which designates the stereochemistry at C7, C8, C9, and C10 of benzo[*a*]pyrene, the modified codon in the *N-ras* protooncogene, and the position of the adducted adenine in this codon (Chart 1).

This work focuses on the solution structure of the SRSR(61,2) adduct. It provides the first example of a (−)-(7*S*,8*R*,9*S*,10*R*)-*N*^{6}-[10-(7,8,9-trihydroxy-7,8,9,10-tetrahy-

[3] The oligonucleotides discussed in this paper do not have terminal phosphate groups—we abbreviate the nomenclature for oligonucleotides by leaving out the phosphodiester linkage. A, C, G, and T refer to mononucleotide units. A right superscript refers to numerical position in the oligonucleotide sequence starting from the 5′-terminus of chain A and proceeding to the 3′-terminus of chain A and then from the 5′-terminus of chain B to the 3′-terminus of chain B. C2, C5, C6, C8, C1′, C2′, C2″, etc. represent specific carbon nuclei. H2, H5, H6, H8, H1′, H2′, H2″, etc. represent the protons attached to these carbons.

drobenzo[*a*]pyrenyl)]-2′-deoxyadenosyl adduct opposite thymine, in the *ras61* oligodeoxynucleotide. Molecular dynamics calculations using simulated annealing protocols and restrained by ^{1}H nuclear Overhauser effects (Keepers & James, 1984; Havel & Wuthrich, 1985; Wuthrich, 1986; Nilsson et al., 1986; Borgias & James, 1990; Madrid et al., 1991; Mujeeb et al., 1993; Weisz et al., 1994) demonstrate that the pyrenyl moiety intercalates above the 5′-face of the modified adenine from the major groove. A single conformation of the adduct is observed. The rise between C^5•G^{18} and $^{S,R,S,R}A^6$•T^{17} is calculated to be 7 Å. Interstrand stacking between the pyrenyl ring and the T^{17} pyrimidine and G^{18} purine rings is enhanced by the bay ring. Adduct-induced distortion of the double helix is evidenced by buckling of base pairs C^5•G^{18} and $^{S,R,S,R}A^6$•T^{17} and propeller twisting of base pair C^5•G^{18}. The work extends the pattern for adenine N6 benzo[*a*]pyrene adducts, in which the *R* stereochemistry at C10 predicts 5′-intercalation of the pyrenyl moiety.

MATERIALS AND METHODS

Materials. The oligodeoxynucleotide 5′-d(CTTCTTGTCCG)-3′ was purchased from the Midland Certified Reagent Co. (Midland, TX). The modified oligodeoxynucleotide 5′-d(CGGAC^{S,R,S,R}AAGAAG)-3′ (Chart 1) was synthesized through a nonbiomimetic procedure in which (±)-amino triol derived from (±)-7β,8α-dihydroxy-9α,10α-epoxy-7,8,9,10-tetrahydrobenzo[*a*]pyrene [(±)-DE2] was reacted with an oligodeoxynucleotide containing 6-fluoroadenosine at position X^6 (Kim et al., 1991, 1992; Harris et al., 1994). The modified oligodeoxynucleotide was purified by HPLC using a reverse-phase semipreparative column (PRP-1; Hamilton Co., Reno, NV) equilibrated with 10 mM ethylenediamineacetate (pH 7.0). The oligodeoxynucleotide was eluted using a gradient consisting of 0−20% acetonitrile in 20 min. The DNA was lyophilized and desalted on Sephadex G-25 (Pharmacia-PL Biochemicals, Inc., Piscataway, NJ).

Preparation of NMR Samples. The concentrations of the single-stranded oligodeoxynucleotides 5′-d(CTTCTTGTCCG)-3′ and 5′-d(CGGAC^{S,R,S,R}AAGAAG)-3′ were determined from the calculated extinction coefficients, 1.09×10^5 and 9.24×10^4 M^{-1} cm^{-1}, respectively (Borer, 1975). The complementary oligodeoxynucleotides were mixed in equal molar proportion in 10 mM NaH_2PO_4, 0.1 M NaCl, and 50 μM Na_2EDTA, at pH 6.9. The mixture was heated to 85 °C for 5 min, followed by cooling to room temperature to anneal the strands. DNA grade Bio-Gel hydroxylapatite (Bio-Rad Laboratories, Richmond, CA) (15 cm × 3.0 cm), eluted with a gradient from 10 to 200 mM NaH_2PO_4 (pH 6.9), was used for the separation of double- from single-stranded oligodeoxynucleotides. The duplex was lyophilized, resuspended in 1 mL of H_2O, and desalted on Sephadex G-25 (70 × 1.5 cm). The sample was lyophilized and dissolved in 0.5 mL of NMR buffer [0.1 M NaCl, 5×10^{-5} M Na_2-EDTA, 0.01 M NaH_2PO_4 (pH 6.9)]. The final strand concentration was determined to be 2.5 mM. Strand stoichiometry was assayed by HPLC.

Nuclear Magnetic Resonance. Spectra were recorded at 500.13 MHz. The sample used for examination of nonexchangeable protons was exchanged three times in 99.96% D_2O and suspended into 0.5 mL of NMR buffer containing 99.996% D_2O. The sample used for examination of exchangeable protons was dissolved in 0.5 mL of NMR buffer containing 9:1 H_2O:D_2O. The spectra were referenced to the water resonance at 4.76 ppm at 20 °C or 4.97 ppm at 10 °C. Phase-sensitive NOESY spectra used for resonance assignments were recorded using the TPPI method for phase cycling. A mixing time of 400 ms was used. In the d_1 dimension, 1024 real data points were collected, with 32 acquisitions per FID with a 1.5 s relaxation delay; 2048 real data points were used in the d_2 dimension. The residual water resonance was saturated during the relaxation delay and the mixing period. Data were zero-filled in the d_1 dimension to give a matrix of 2K × 2K real points. A sine-bell apodization function with a 90° phase shift and a skew factor of 0.7 was used in the d_1 and d_2 dimensions. Phase-sensitive NOESY experiments in 9:1 H_2O:D_2O were performed using a jump return 1-1 sequence for water suppression as the read pulse (Bax et al., 1987; Sklenar et al., 1987). Convolution difference was used during processing to minimize the residual water signal (Marion et al., 1989). The NOE mixing time was 250 ms. In the d_1 dimension, 512 data points were collected, with 64 scans per FID; the relaxation delay was 1.5 s. In the d_2 dimension, 2K data points were utilized. These experiments were carried out at 10 °C. Phase-sensitive TOCSY spectra were recorded at 20 °C using a 105 ms MLEV17 (Bax & Davis, 1985) spin lock at 2 G for mixing (phase cycling was done according to the TPPI method). All NMR data were transferred to Iris 4D workstations (Silicon Graphics, Inc., Mountain View, CA) and processed using FELIX (Biosym Technologies, San Diego, CA).

NMR Distance Restraints. Classical B-DNA and A-DNA (Arnott & Hukins, 1972) were used as the reference structures. The initial DNA models were constructed by bonding C10 of BPDE to N6 of adenine, with the correct stereochemistry. Partial charges on the benzo[*a*]pyrene moiety were obtained from Hingerty et al. (1989). These were energy minimized for 500 iterations by the conjugate gradient method to give the starting structures used in the MD calculations. NOESY spectra at mixing times of 200, 300, and 400 ms were acquired within a single 3-day period without removing the sample from the spectrometer or changing the experimental conditions. The NOESY pulse program was modified to eliminate artifacts arising from zero-quantum coherence and *zz* terms observed at short mixing times. A systematically shifted composite 180° pulse was implemented within the mixing period, and composite 90° pulses were used in place of the second and third 90° pulses in the standard pulse sequence (Bodenhausen et al., 1984). Footprints were drawn around the NOE cross-peaks for the NOESY spectrum measured at a mixing time of 400 ms using FELIX. The same set of footprints was applied to spectra measured at other mixing times. Cross-peak intensities were determined by volume integration of the areas under the footprints. The intensities were combined as necessary with intensities generated from complete relaxation matrix analysis of a starting DNA structure to generate a hybrid intensity matrix. MARDIGRAS (Borgias & James, 1990) was used to iteratively refine the hybrid matrix. Calculations using three DNA starting models generated by INSIGHTII (Biosym Technologies, San Diego, CA), three mixing time NOE experiments, and a DNA correlation time of 5 ns yielded nine sets of distances which were averaged to give the experimental NOE restraints used in the molecular dynamics calculations.

Molecular Dynamics and Simulated Annealing. INSIGHTII was used to build the starting structures and for

molecular visualization. All potential energy minimization and restrained MD calculations were performed using X-PLOR (Brunger, 1992). This was derived from CHARMM (Brooks et al., 1983) and adapted for restrained MD calculations of nucleic acids. The empirical energy function (Nilsson et al., 1986) was developed especially for nucleic acids and treated all hydrogens explicitly. It consisted of energy terms for bonds, bond angles, torsion angles, tetrahedral and planar geometry, hydrogen bonding, and nonbonded interactions including van der Waals and electrostatic forces. The van der Waals energy term was approximated using the Lennard-Jones potential energy function. The electrostatic term used the Coulomb function, based on a full set of partial charges (−1/residue) and a distance-dependent dielectric constant of 4. The nonbonded pair list was updated if any atom moved more than 0.5 Å, and the cutoff radius for nonbonded interactions was 11 Å. The effective energy function was composed of two terms describing distance and dihedral restraints, which were in the form of a square well potential (Clore et al., 1986). All bond lengths involving hydrogen were kept fixed with the SHAKE algorithm (Ryckaert et al., 1977) during MD calculations. All calculations were performed *in vacuo* without explicit counterions. The integration time step used in the molecular dynamics calculations was 1 fs. Structure coordinates were archived every 0.1 ps. Back-calculation of NMR data was performed using CORMA (Keepers & James, 1984). The refined structures were analyzed using DIALS AND WINDOWS 1.0 (Ravishankar et al., 1989).

RESULTS

Melting Studies. The thermal stability of the adduct was examined by UV melting studies which compared it with the unadducted *ras61* sequence. The adduct destabilized the duplex, as indicated by a 13 °C reduction in T_m. A series of 1D ^{1}H spectra obtained at temperatures from 5 to 45 °C indicated 20 °C to be the optimal temperature at which the duplex remained intact and the ^{1}H resonances were the sharpest and best resolved.

^{1}H Resonance Assignments. (a) Nonexchangeable Protons. Figure 1 shows the sequential assignment schemes for the modified and the complementary strands (Hare et al., 1983; Feigon et al., 1983). For the modified strand, weaker NOE connectivities than for a normal B-DNA base step were observed between A^4 H1′ and C^5 H6 and between C^5 H1′ and $^{S,R,S,R}A^6$ H8. The intranucleotide NOE between C^5 H1′ and C^5 H6 was weaker than observed in B-DNA. NOE connectivities for the remainder of the modified strand had intensities as expected for B-DNA. In the complementary strand, the internucleotide connectivity between T^{16} H1′ and T^{17} H6 was weaker than the corresponding NOEs observed for nucleotides far from the site of the lesion. No connectivity was observed between T^{17} H1′ and G^{18} H8. The intranucleotide NOEs between H1′ and base protons for T^{16} and for G^{18} were weaker than corresponding NOEs for nucleotides far from the site of the lesion. The strength of the intranucleotide NOE between T^{17} H1′ and H6 could not be assessed, due to the fact that it was close to the diagonal. Figure 1C shows an expanded plot from a TOCSY spectrum. Five of the six cytosines displayed cross-peaks in the expected region. The sixth, assigned to C^5, revealed a 1 ppm upfield shift of H5 relative to that normally observed for cytosine H5 protons. C^5 H6 also shifted upfield. Another large upfield shift was observed for T^{17} H6, which was at 6.2 ppm as compared to the usual 7−7.2 ppm range.

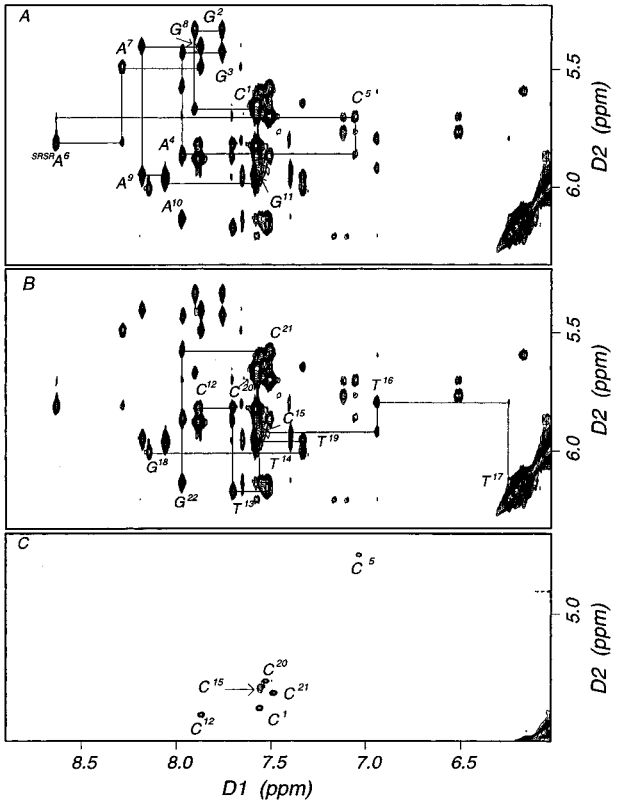

FIGURE 1: Expanded plots from a NOESY spectrum at 400 ms mixing time and a TOCSY experiment with a 105 ms spin lock. (A) The aromatic−anomeric region of the NOESY spectrum showing the NOE sequential assignment scheme for the modified strand. (B) The aromatic−anomeric region of the NOESY spectrum showing the NOE sequential assignment scheme for the unmodified strand. (C) The aromatic−anomeric region of the TOCSY spectrum showing cytosine H5−H6 scalar couplings. Both experiments were at 20 °C.

The assignments of the H2′ and H2″ sugar protons were obtained from their connectivities with the H1′ protons of the same nucleotides, based upon the assumption that, for B-like DNA, the H1′−H2″ distances were shorter than the H1′−H2′ distances. Therefore, the stronger cross-peaks were assigned to the H2″ protons. Where nearly isochronous resonances were observed for the H2′ and H2″ protons, NOEs between the base and H2′/H2″ protons discriminated between the two resonances. The assignments of the remainder of the sugar protons were determined from TOCSY spectra. The H5′/H5″ resonances were in most cases overlapped, making their unambiguous assignments impossible. The adenine H2 protons were assigned from weak cross-peaks to the H1′ protons of the adjacent 3′-nucleotides. Table S1 in the Supporting Information lists the chemical shifts of the nonexchangeable protons.

(b) Exchangeable Protons. Assignments of the imino and amino protons were made from NOESY spectra measured in 90% H_2O at 10 °C (Boelens et al., 1985). An expanded region showing cross-peaks between the imino protons is given in Figure 2. A total of 10 well-resolved imino resonances were observed, five of which displayed sharp peaks. Sequential assignments of the imino protons from base pairs G^2·C^{21} → C^5·G^{18} and A^7·T^{16} → A^{10}·T^{13} were obtained unequivocally. The imino protons of the terminal base pairs were broadened, probably due to increased exchange with solvent. The imino proton of base pair

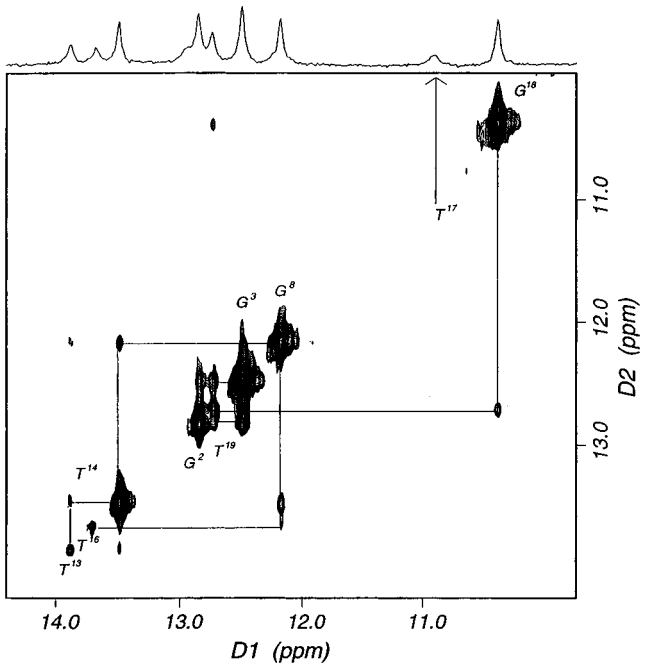

FIGURE 2: An expanded plot of a NOESY spectrum at 250 ms mixing time showing the sequential NOE connectivities for the imino protons of base pairs $G^2 \cdot C^{21} \rightarrow A^{10} \cdot T^{13}$. The labels represent the imino proton of the designated base. Also shown is a 1D projection of the imino proton resonances. Both 1D and 2D experiments were at 10 °C.

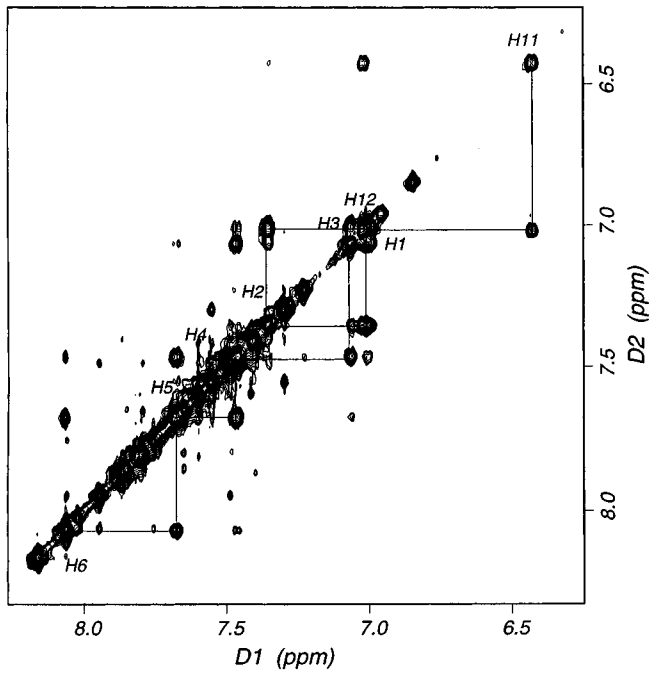

FIGURE 3: An expanded NOESY spectrum of the aromatic−aromatic region at 400 ms mixing time, showing the sequential assignment scheme for the aromatic protons of benzo[*a*]pyrene. The experiment was at 20 °C.

$A^{10} \cdot T^{13}$ was broadened, as was that of base pair $A^7 \cdot T^{16}$. An upfield-shifted and broadened resonance at 10.9 ppm was observed in the 1D projection but not in the 2D contour plot. It was assigned to $^{S,R,S,R}A^6 \cdot T^{17}$ on the basis of an NOE connectivity with $^{S,R,S,R}A^6$ H2. The broadening of T^{16} and T^{17} N3H was consistent with the 13 °C lower T_m as compared to the unadducted *ras61* duplex. Although T^{16} N3H was broadened, a NOE was still observed between this resonance and G^8 N1H, its 5′-neighbor imino proton. No NOE connectivities were observed between T^{17} N3H and its 3′- or 5′-neighboring base pairs. Other features were large upfield shifts for T^{17} N3H and G^{18} N1H (located at 10.5 and 10.9 ppm, respectively), in comparison to the corresponding resonances of the unadducted duplex (12.3 and 13.8 ppm, respectively) (Feng & Stone, 1995).

The non-hydrogen-bonded amino protons of cytosine (NH_{2a}) were assigned from their intranucleotide connectivities to cytosine H5 protons. The hydrogen-bonded amino protons of cytosines (NH_{2b}) were assigned from their intranucleotide cross-peaks to NH_{2a} resonances. With the exception of the 5′-terminal C^1 and C^{12} nucleotides, distinctive amino resonances were observed for each cytosine, including C^5, the 5′-neighbor to the site of adduction. The guanine amino protons exchanged with solvent at an intermediate rate on the NMR time scale, which rendered their assignment impossible. The adenine amino protons were also not assigned due to exchange broadening. Upfield shifts of 1.3 ppm for NH_{2a} and 1.6 ppm for NH_{2b} were observed for C^5 relative to the chemical shifts observed for these resonances in the unmodified *ras61* duplex (Feng & Stone, 1995). No unusual shifts were observed for the amino protons of other cytosines. The chemical shifts of the exchangeable protons are listed in Table S2 in the Supporting Information.

(c) Benzo[a]pyrene Protons. The benzo[*a*]pyrene resonances were assigned from NOESY and TOCSY spectra at 20 °C. An expanded region of the NOESY spectrum used for the assignment of pyrenyl protons is shown in Figure 3. The numbering scheme for the benzo[*a*]pyrene protons is shown in Chart 1. The aliphatic ring resonances were assigned from connectivities (1) to benzo[*a*]pyrene H6 and H11, (2) within the aliphatic ring, and (3) with DNA resonances. A strong NOE was found between benzo[*a*]-pyrene H6 and a resonance at 5.76 ppm. This was assigned to H10. A weak cross-peak was detected between H10 and a resonance at 3.83 ppm. This was assigned to H9. A weak NOE but strong TOCSY cross-peak was detected between H9 and a resonance at 4.50 ppm. The latter resonance was assigned to H8. H7 was assigned from connectivities to C^5 H5, and it resonated at 5.16 ppm. No connectivities were detected between H7, H8, or H9. However, a weak NOE was detected between H10 and H8. The chemical shifts of the pyrenyl and aliphatic ring resonances are listed in Table S3 in the Supporting Information.

Benzo[a]pyrene−DNA NOEs. A total of 46 NOEs were found between the benzo[*a*]pyrene and DNA protons. A number of these are shown in Figure 4. The benzo[*a*]pyrene aromatic protons H3−H6 exhibited moderate-to-strong cross-peaks to T^{17} CH_3. Benzo[*a*]pyrene H1, H3 and H4 showed cross-peaks to T^{17} H2′,H2″. In addition, H1−H4 showed weak cross-peaks to T^{17} H6. Cross-peaks were observed between H11 and H12 and between C^5 H2′,H2″ and C^5 H1′. A cross-peak was observed between H10 and C^5 H6. Weak cross-peaks were observed between H4 and T^{19} CH_3 and between H6 and T^{16} CH_3. Cross-peaks were observed between the aromatic resonances of benzo[*a*]pyrene and the exchangeable protons of DNA. The most prominent of these are shown in Figure 4B. These included cross-peaks between G^{18} N1H (the 5′-neighboring base pair to the lesion) and benzo[*a*]pyrene H2−H4, H11, and H12.

Chemical Shift Perturbations. The chemical shifts of the nonexchangeable and exchangeable protons, compared to the unmodified *ras61* sequence, are shown in Figure 5. The

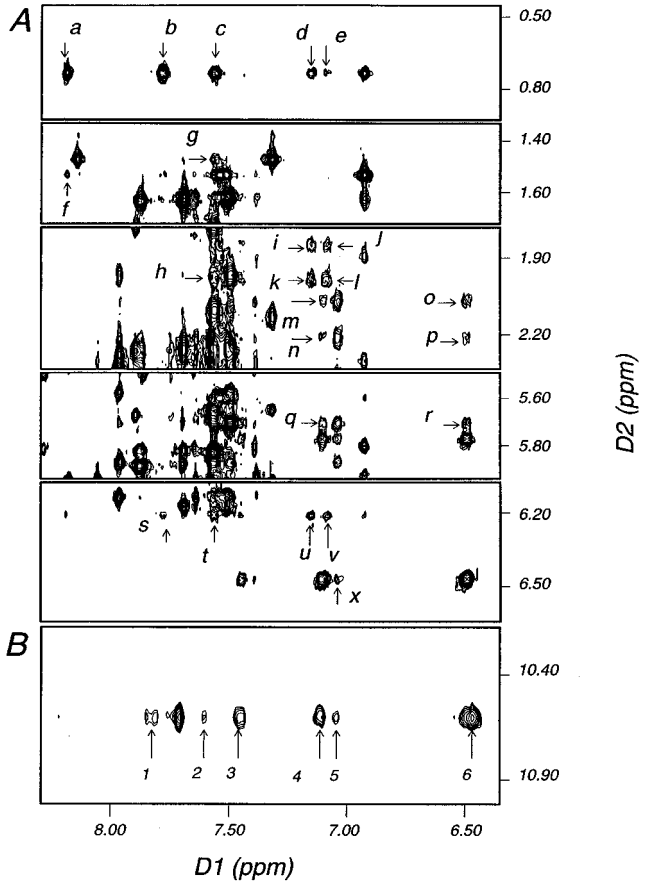

FIGURE 4: Tile plots showing NOE cross-peaks between DNA and benzo[*a*]pyrene protons. (A) Cross-peaks: a, T^{17} CH_3 → H6; b, T^{17} CH_3 → H5; c, T^{17} CH_3 → H4; d, T^{17} CH_3 → H3; e, T^{17} CH_3 → H1; f, T^{19} CH_3 → H6; g, T^{16} CH_3 → H4; h, T^{17} H2″ → H4; i, j, T^{17} H2′ → H3, H1; k, l, T^{17} H2″ → H1, H3; m−p, C^5 H2′, H2″ → H12, H11; q, r, C^5 H1′ → H12, H11; s−v, T^{17} H6 → H2, H4, H3, and H1; x, C^5 H6 → H10. (B) Cross-peaks: 1−6, G^{18} N1H → H5, H4, H2, H3, H1, and H11.

greatest upfield shift (2.6 ppm) was observed for T^{17} N3H, the imino proton of the adducted base pair. The imino proton of C^5•G^{18} also experienced an upfield shift of 1.8 ppm. C^5 NH_{2b} shifted upfield 1.6 ppm. Upfield chemical shift changes of 1 ppm were observed for T^{17} H6 and CH_3 and T^{16} H2′,H2″. A 0.75 ppm upfield shift was detected for C^5 H5. Other smaller upfield shifts were observed for a number of protons near the adduction site. These included T^{16} H6 (0.6 ppm), T^{17} H2″ (0.55 ppm), A^4 H1′, H2′, and H2″ (0.3−0.4 ppm), and A^7 H1′ (0.3 ppm).

Structural Refinement. Stereoviews of the three starting structures are shown in Figure S1 in the Supporting Information. Relaxation matrices generated from the three starting structures used an isotropic correlation time of 5 ns for both sugar and base protons, derived from τ_c measured from fluorescence anisotropy. A total of nine distance sets, each consisting of 402 restraints, were generated. After the removal of poor distances that resulted from overlapped NOE intensities or the water presaturation pulse, the nine sets of distance restraints were averaged, resulting in a total of 369 internuclear distances. Of these distances, 231 were intranucleotide restraints, 100 were interresidue restraints, and 38 were benzo[*a*]pyrene−DNA restraints. An average of 36 experimental NOE restraints were obtained for each base pair. The distribution of these restraints for each base is summarized in Table 1. The distribution of NOE restraints was not equal for all bases. With the exception of G^8, all

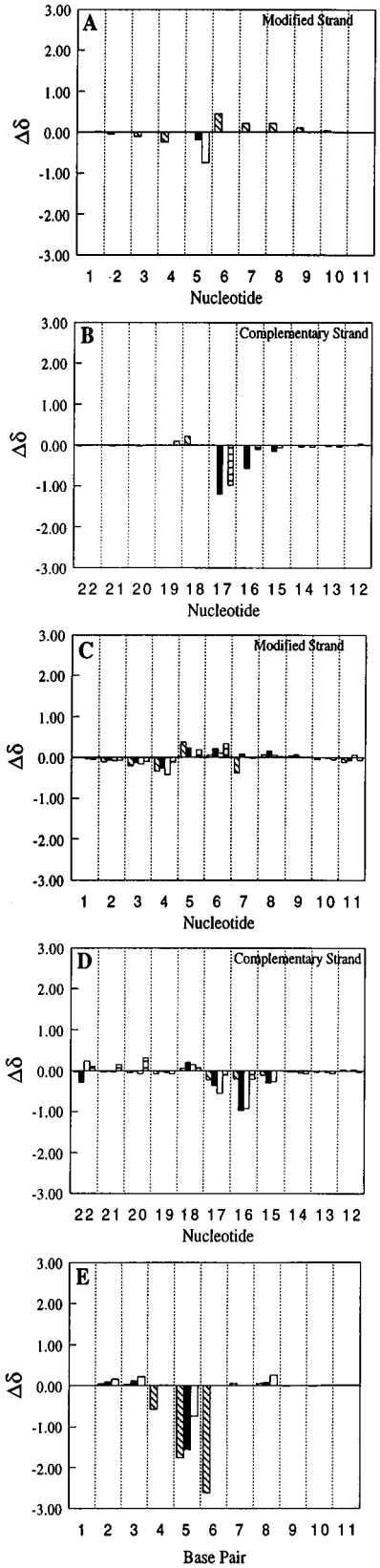

FIGURE 5: Chemical shift changes of selected protons relative to the unmodified *ras61* duplex. Panels A and B: major groove protons in the modified and complementary strands, respectively. Cross-hatched bars, G H8 or A H8; open bars, C H5; solid bars, C H6 and T H6; horizontal-line bars, T CH_3. Panels C and D: minor groove protons in the modified and complementary strands, respectively. Cross-hatched bars, H1′; solid bars, H2′; open bars, H2″; horizontal bars, H3′. Panel E: exchangeable protons. Cross-hatched bars, G N1H and T N3H; solid bars, C N4H(b); open bars, C N4H(a). Positive $\Delta\delta$ values indicate upfield shifts relative to the *ras61* oligodeoxynucleotide. $\Delta\delta = [\delta_{\text{unmodified oligomer}} - \delta_{\text{modified oligomer}}]$ (ppm).

Table 1: Distribution of Experimental Restraints among Nucleotide Units for the SRSR(61,2) Adduct

nucleotide	intranucleotide restraints	internucleotide restraints[a]	total exptl restraints
C^{1}	15		15
G^{2}	9	5	14
G^{3}	6	2	8
A^{4}	8	2	10
C^{5}	14	9	23
$^{S,R,S,R}A^{6}$	11	6	17
A^{7}	15	5	20
G^{8}	2	3	5
A^{9}	10	4	14
A^{10}	6	3	9
G^{11}	12	5	17
C^{12}	16	0	16
T^{13}	11	9	20
T^{14}	6	7	13
C^{15}	11	7	18
T^{16}	21	10	31
T^{17}	10	12	22
G^{18}	18	0	18
T^{19}	8	6	14
C^{20}	5	7	12
C^{21}	10	5	15
G^{22}	7	5	12

[a] The internucleotide NOEs are listed in the direction $n \rightarrow n - 1$.

Table 2: Comparison of Sixth Root Residual Indices R_1^x for Starting Models and Resulting MD Structures[a−c]

	intranucleotide R_1^x	internucleotide R_1^x	overall R_1^x
BP-Ao	15	20	16
BP-Bo	9.0	20	13
BP-Bi	8.0	15.5	10.8
⟨MDAo⟩	8.2	11.5	8.7
⟨MDBo⟩	7.8	11.0	8.5
⟨MDBi⟩	7.2	11.0	8.4
⟨rMDav⟩	7.2	10.0	8.1

[a] Only the inner nine base pairs were used in the calculations, to exclude end effects. The mixing time was 400 ms. [b] $R_1^x = \sum|(a_o)_i^{1/6} - (a_c)_i^{1/6}|/\sum|(a_o)_i^{1/6}|$, where (a_o) and (a_c) are the intensities of observed (non-zero) and calculated NOE cross-peaks. [c] BP-Ao, starting energy-minimized A-DNA with the BP moiety situated in the major groove; BP-Bo, starting energy-minimized B-DNA with the BP moiety situated in the major groove; BP-Bi, starting energy-minimized B-DNA with the BP moiety intercalated between base pairs 5 and 6; <MDAo>, average of six rMD structures starting from BP-Ao; <MDBo>, average of six MD structures starting from BP-Bo; <MDBi>, average of six MD structures starting from BP-Bi; <rMDav>, average of 18 rMD structures starting from BP-Ao, BP-Bo, and BP-Bi.

bases had five or more intranucleotide NOEs. However, C^{3}, A^{4}, G^{8}, A^{9}, A^{10}, and G^{18} were underparametrized with respect to interbase NOEs (each possessed fewer than five interbase NOEs). A list of NOE-generated distances along with the upper and lower bounds is shown in Table S4 of the Supporting Information.

Refined Structure. Three starting structures were used. One was built such that the adducted benzo[*a*]pyrene moiety was situated in the B-DNA major groove (designated BP-Bo); the second was built from B-DNA such that the adducted benzo[*a*]pyrene moiety intercalated between C^{5}•G^{18} and $^{S,R,S,R}A^{6}$•T^{17} (designated BP-Bi); the third structure was built such that the adducted benzo[*a*]pyrene moiety was situated in the A-DNA major groove (designated BP-Ao). Stereoviews of these starting structures are shown in Figure S1 in the Supporting Information. Figure 6 shows stereoviews of six MD-generated structures based on BP-Bo, BP-Bi, and BP-Ao. The final structures obtained by averaging each family of emergent structures, followed by PEM, are shown in Figure 7. These were averaged and energy minimized to obtain the structure <rMDav>, a space-filling model of which is shown in Figure 8.

The precision of the emergent structures was monitored by pairwise calculation of rms deviations (rmsd) (Figure 9). The BP-Ao starting structure was different from either BP-Bo or BP-Bi, evidenced by a rmsd of 10 Å. BP-Bo and BP-Bi were similar, with a rmsd of 2 Å. A site-specific increase in rmsd between BP-Bo and BP-Bi, to 4 Å, was localized at $^{S,R,S,R}A^{6}$. The BP-Ao starting structure was different from <rMDav>, with a rmsd of 10 Å, which indicated that the emergent structures did not converge to an A-DNA geometry. When compared to <rMDav>, the BP-Bo and BP-Bi starting structures each yielded a rmsd of 2 Å, suggesting that the emergent structures converged toward B-DNA geometry. The average rmsds between the refined structure, <rMDav>, and <rMDA>, <rMDBo>, and <rMDBi> were <1 Å. MD calculations performed using the three starting structures in the absence of the NOE restraints did not converge, which indicated that the convergence to the final structures shown in Figure 7 was due to the NOE restraints.

The accuracy of the emergent structures was assessed by complete relaxation matrix calculations, which compared theoretical NOE intensities generated from the model structures with experimental data. Table 2 shows sixth root R_1^x factors for the inner nine base pairs of the starting structures and the refined structures emergent from MD. The R_1^x factors $>15 \times 10^{-2}$ for internucleotide NOEs indicated that each of the starting structures was inconsistent with the data, although from the B-form starting structures BP-Bo and BP-Bi, the latter gave reasonable R_1^x values of 8.0×10^{-2} for intranucleotide NOEs. In contrast, theoretical NOE intensities from each of the refined structures yielded R_1^x values of $(7.2-8.2) \times 10^{-2}$ for intranucleotide NOEs and $(11-11.5) \times 10^{-2}$ for internucleotide NOEs, irrespective of starting structure. Improved values were noted for the structures generated from BP-Bi. In all three instances, poorer convergence was obtained for the interbase NOEs. Examination of Table S4 in the Supporting Information and CORMA output files indicated that submatrices representing the nucleotides which were under-represented by internucleotide NOEs (<4 NOEs/nucleotide) gave poorer R_1^x values. The nucleotides at and near the site of adduction gave good R_1^x values for both intra- and inter-nucleotide NOEs, which suggests that the refined structure is in reasonable agreement with the NOE data, especially near the lesion.

DISCUSSION

The ubiquitous presence of benzo[*a*]pyrene as an environmental pollutant, combined with the mutagenic and carcinogenic properties of the bay-region diol epoxides, has made structural analyses of its DNA adducts a prerequisite step toward understanding benzo[*a*]pyrene-induced carcinogenesis. This work provides the structure of a (−)-(7*S*,8*R*,9*S*,10*R*)-*N*^{6}-[10-(7,8,9,10-tetrahydrobenzo[*a*]pyrenyl)]-2′-deoxyadenosyl adduct at the first adenine of the *N-ras* codon 61, a site at which mutations activate the *N-ras* protooncogene. Obtaining a detailed understanding of the structural perturbations induced in the *ras61* oligomer by BPDE adduction may identify structure−activity relationships which correlate with the biological processing of the resulting adducts.

FIGURE 6: Superposition of (A) the <rMDBi>, (B) the <rMDBo>, and (C) the <rMDAo> families of structures.

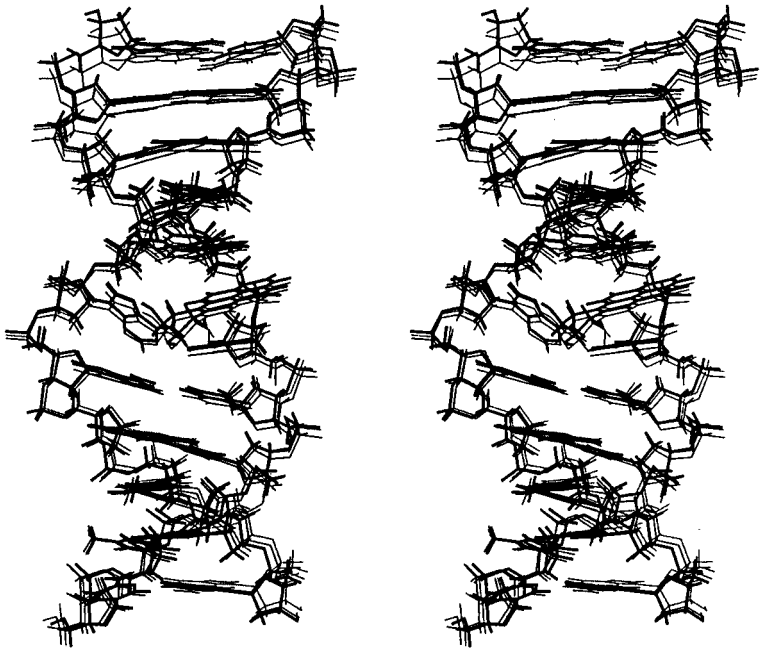

FIGURE 7: Superposition of the energy-minimized average structures for <rMDAo> (narrow line), <rMDBo> (thin bold line), and <rMDBi> (heavy bold line).

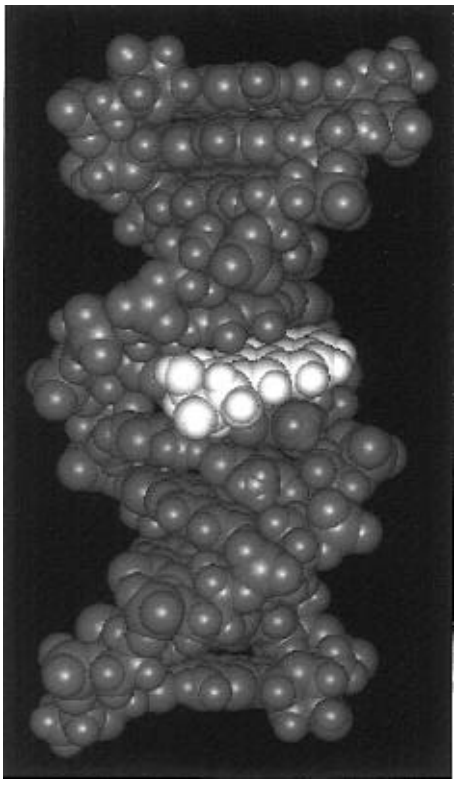

FIGURE 8: CPK representation of the final structure, <rMDav>, averaged from the 18 sets of three families of rMD structures.

Overall Structural Features. Figure 10 shows perpendicular and parallel views through the helical axes for base pairs C^5·G^{18} and $^{S,R,S,R}A^6$·T^{17} as compared to C^5·G^{18} and A^6·T^{17} of the *ras61* duplex. The pyrenyl moiety intercalated from the major groove of the DNA and above the 5′-face of the modified adenine. The pyrenyl ring did not completely thread the DNA helix; thus we describe this as "quasi-intercalated" geometry, from the major groove. Nevertheless, the stacking interactions between the pyrenyl ring and the DNA bases clearly distinguished this as an intercalated as opposed to a major groove adduct. Strong interstrand stacking occurred between the pyrenyl ring and the T^{17} pyrimidine and G^{18} purine rings, in the complementary strand. Stacking was enhanced by the bay-region ring of the pyrenyl moiety. In contrast, poor stacking was observed between the pyrenyl moiety and C^5 and $^{S,R,S,R}A^6$ in the modified strand. Both of these bases were twisted, presumably to alleviate steric clashes with the hydroxyl groups of the benzo[*a*]pyrene, which faced into the major groove. Modification of the conformations of base pairs C^5·G^{18} and $^{S,R,S,R}A^6$·T^{17} disrupted Watson−Crick base-pairing geometries, suggesting weakened hydrogen bonding. Helicoidal analysis suggested a +30° change in buckle for C^5·G^{18} and a −25° change in buckle for $^{S,R,S,R}A^6$·T^{17}, relative to the unmodified *ras61* oligomer. A −40° change in propeller twist for C^5·G^{18} was observed. The rise between base pairs C^5·G^{18} and $^{S,R,S,R}A^6$·T^{17} was 7 Å as compared to the value of 3.5 Å normally observed for B-DNA.

The emergent structure was consistent with the NOE data. The expected NOE connectivity between the neighboring imino protons in base pairs C^5·G^{18} and $^{S,R,S,R}A^6$·T^{17} was missing, which in combination with the observed pattern of DNA−benzo[*a*]pyrene NOEs confirmed intercalation between these two base pairs. The orientation of the benzo[*a*]pyrene ring resulted in localization of the NOEs between the adduct and DNA on the two faces of the pyrenyl ring. The benzo[*a*]pyrene aromatic protons H3−H6 faced toward the major groove and exhibited NOEs to T^{17} CH_3, located below the major groove face of the pyrenyl moiety. The intercalation of the pyrenyl moiety oriented H1, H2, and H3 toward the deoxyribose of T^{17} in the complementary strand; these protons and H4 showed NOEs to T^{17} H2′,H2″ and to T^{17} H6. NOEs between H11 and H12 and between C^5 H2′,H2″ and C^5 H1′ were explained by the location of the bay ring beneath C^5. The imino proton G^{18} N1H was directly above the pyrene ring and showed NOEs to both faces of

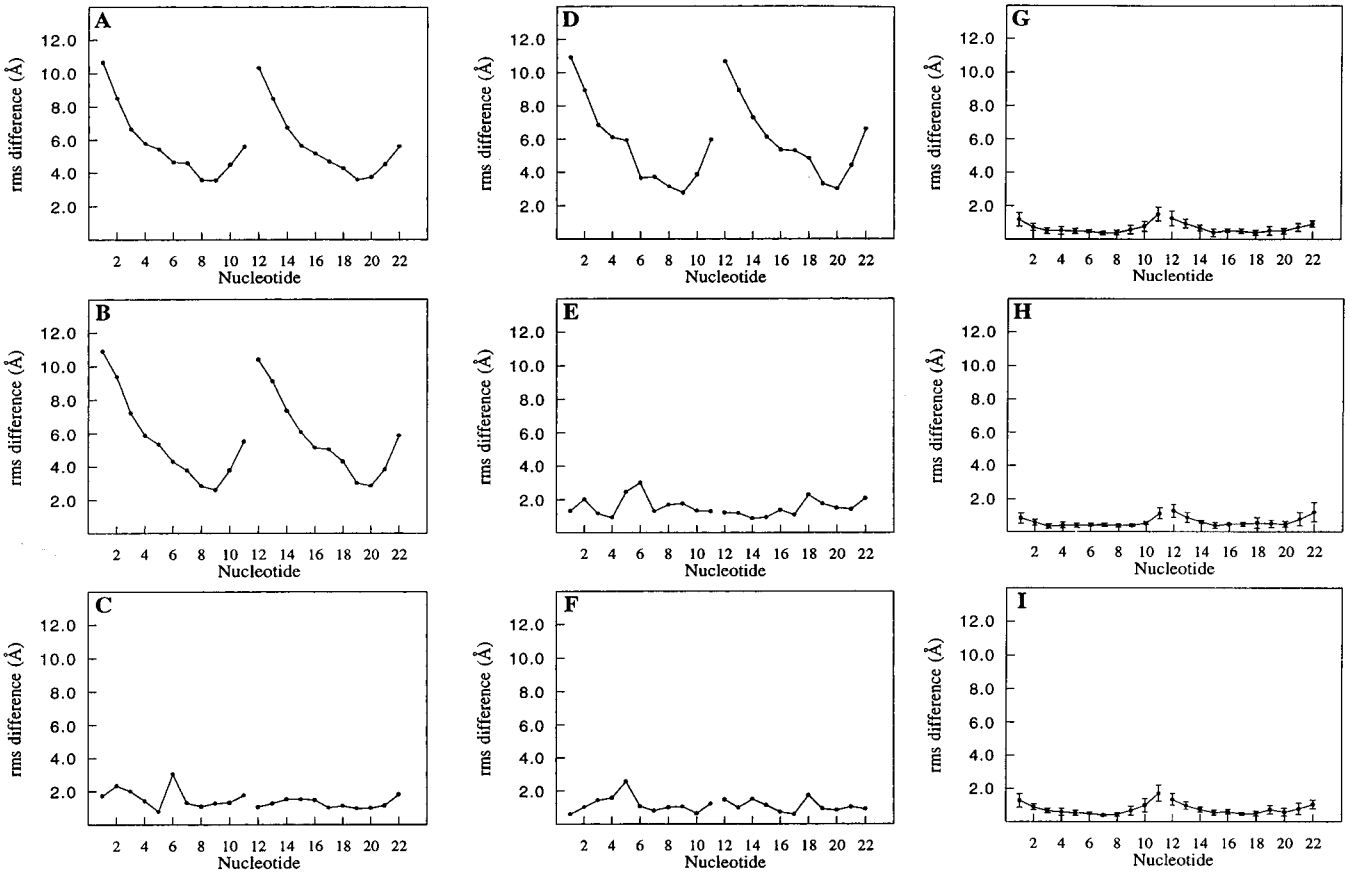

FIGURE 9: Per residue rmsd comparisons between the initial structures and the final structures. Panels: (A) rBP-Ao vs rBP-Bo; (B) rBP-Ao vs rBP-Bi; (C) rBP-Bo vs rBP-Bi; (D) rBP-Ao vs <rMDav>; (E) rBP-Bo vs <rMDav>; (F) rBP-Bi vs <rMDav>; (G−I) <RMDAo>, <rMDBo>, and <rMDBi> vs <rMDav>, respectively. The error bars represent standard deviations. The slopes of the lines result from the reference frame in these calculations.

the benzo[*a*]pyrene (the aromatic protons H2−H4, H11, and H12).

The 1.5 ppm dispersion of the benzo[*a*]pyrene aromatic proton chemical shifts was striking and was consistent with intercalation of the PAH. This indicated that the pyrenyl moiety was in a less homogeneous environment than would have been expected if it were situated in the major groove. The orientation of the pyrenyl moiety explained the upfield chemical shifts of 1 ppm, observed for T^{17} H6 and CH_3. These protons both lay beneath the PAH ring. The 0.75 ppm upfield shift for C^5 H5 was explained by its orientation near the edge of the pyrenyl moiety. The smaller shift observed for C^5 H6 was explained by its orientation above the saturated ring of benzo[*a*]pyrene. The upfield shifts of the exchangeable protons of base pairs $C^5{\cdot}G^{18}$ and $^{S,R,S,R}A^6{\cdot}T^{17}$ supported the notion that benzo[*a*]pyrene was intercalated toward the 5′-direction from the lesion. The most dramatic upfield shift was 2.6 ppm for T^{17} N3H, the imino proton of the adducted base pair. This proton was stacked under the bay-region ring of the pyrenyl moiety. The large shift of this proton perhaps indicates that the geometry shown in Figure 10, which emerged from the NOE-restrained MD calculations, does not have the pyrenyl ring inserted quite far enough into the helix. Further insertion of the aromatic moiety into the helix seems reasonable, especially since it should enhance stacking interactions between the PAH aromatic ring and the neighboring nucleotides. The imino proton of $C^5{\cdot}G^{18}$ shifted upfield 1.8 ppm, and C^5 NH_{2b} shifted upfield 1.6 ppm, also consistent with the stacking interaction shown in Figure 10. Chemical shift perturbations indicated that BPDE adduction altered the electronic environment of the DNA protons up to two base pairs in the 5′-direction and one base pair in the 3′-direction from the lesion. Smaller upfield shifts observed for a number of other protons near the adduction site probably also resulted from the ring current of the pyrenyl moiety.

Thermal destabilization of the $^{S,R,S,R}A^6$-modified DNA duplex occurred despite the intercalation of the benzo[*a*]pyrene moiety into the helix and favorable stacking with T^{17} and G^{18}. Thus, stacking interactions between the benzo[*a*]pyrene and T^{17} and G^{18} bases were offset by adduct-induced conformational distortion of the double helix at the lesion site, with disruption of H-bonding at $^{SRSR}A^6{\cdot}T^{17}$. This differed from physical (noncovalent) binding of pyrene and benzo[*a*]pyrene derivatives to DNA, which preferred duplex DNA, presumably due to favorable stacking which stabilized the duplex (Wolfe et al., 1987). Thermal destabilization of duplex oligodeoxynucleotides was observed for other benzo[*a*]pyrene (Lakshman et al., 1992; Schurter et al., 1995a,b; Yeh et al., 1995; Fountain & Krugh, 1995; Mao et al., 1995) adducts.

An interesting feature was the broadening of C^5 H5 and H6 (Figure 2A). On the benzo[*a*]pyrene moiety, H8 and H9 were broadened, but H7 and H10 were sharp. The intensity of G^{18} N1H of the $C^5{\cdot}G^{18}$ base pair suggested that broadening of C^5 H5 and H6 did not result from transient opening. We speculated that the benzo[*a*]pyrene aliphatic ring, directly under C^5 H5 and H6, equilibrated about the C8−C9 bond between two half-chair conformations. The half-chair conformation, considered to be more energetically favorable (Schurter et al., 1995a,b), positioned the C7 and C8 hydroxyls pseudoaxial and placed the H8−H10 and H7−

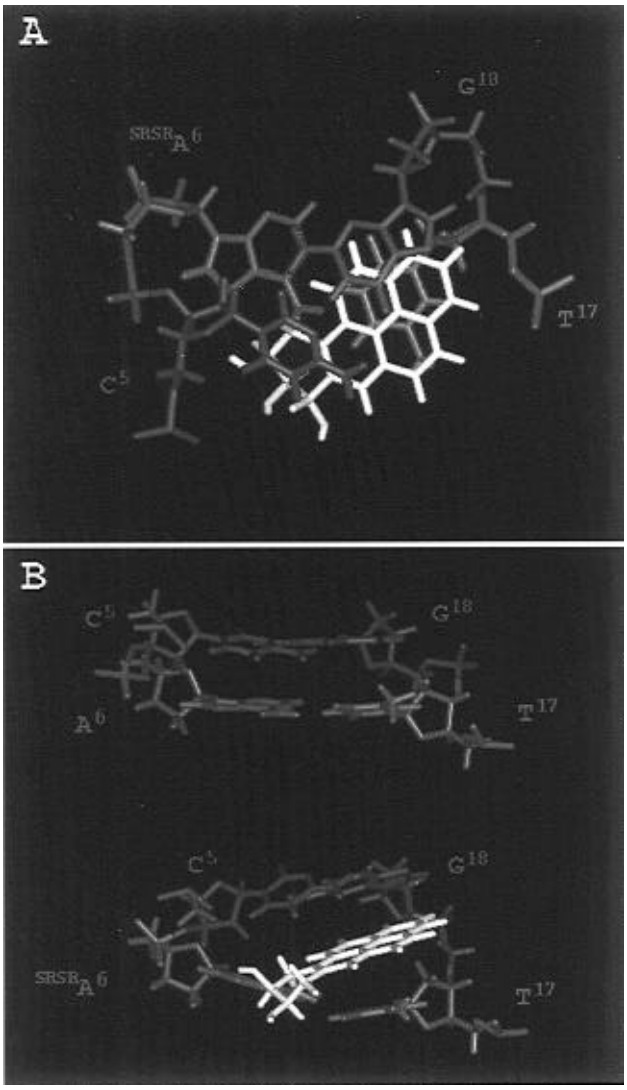

FIGURE 10: (A) Stacking patterns of the $C^5 \cdot G^{18}$ base pair above $^{S,R,S,R}A^6 \cdot T^{17}$. B. Views of (top) base pairs $C^5 \cdot G^{18}$ and $A^6 \cdot T^{17}$ in the unmodified *ras61* oligomer and (bottom) base pairs $C^5 \cdot G^{18}$ and $^{S,R,S,R}A^6 \cdot T^{17}$ from the major groove.

H9 pairs >5 Å apart, which is consistent with the lack of strong NOEs between these protons.

Stereochemistry at C10 of Benzo[a]pyrene. The present work extends the pattern for adenine N6 benzo[*a*]pyrene adducts, in which the stereochemistry at C10 seems to be the crucial determinant of 5′-intercalation of the pyrenyl moiety (Schurter et al., 1995b). All C10*R* isomers examined to date intercalate toward the 5′-direction. The present structure is similar to that observed for a (−)-(7*R*,8*S*,9*R*,-10*R*)-*N*^{6}-[10-(7,8,9,10-tetrahydrobenzo[*a*]pyrenyl)]-2′-deoxyadenosyl adduct with dT opposite the lesion (Schurter et al., 1995a). That structure corresponded to an adduct from the syn (−)-DE1. The diastereomeric benzo[*c*]phenanthrene adducts also followed this pattern, with C1 (the adducted carbon) stereochemistry being crucial (Cosman et al., 1993b).[4]

A significant difference was noted between the (−)-(7*S*,8*R*,9*S*,10*R*)-*N*^{6}-[10-(7,8,9,10-tetrahydrobenzo[*a*]pyrenyl)]-2′-deoxyadenosyl adducts examined in this study, and opposite dG (Schurter et al., 1995b; Yeh et al., 1995), the diastereomeric benzo[*c*]phenanthrene adducts (Cosman et al., 1994a, 1995a), the (−)-7*R*,8*S*,9*R*,10*R*)-*N*^{6}-[10-(7,8,9,10-tetrahydrobenzo[*a*]pyrenyl)]-2′-deoxyadenosyl adduct opposite dT, and the styrene oxide adducts at adenine N6 (Feng et al., 1995, 1996). In each instance, the PAH adduct intercalated, while the styrene oxide adducts were located in the major groove. This may occur due to greater stacking affinity of the planar polycyclic ring in the PAH compounds. Another contributing factor could be the facile rotation of the styrene oxide adducts about the linkage between the benzylic carbon and the phenyl ring, which is not accessible to the PAH compounds.

Comparison to Adduct-Directed Mutagenesis Studies. In vivo site-directed mutagenesis experiments performed on the SRSR(61,2) adduct and two additional 10*R* and three additional 10*S* stereoisomers of BPDE adducts at the *ras61* (61,2) locus showed that each generated A → G mutations, at frequencies ranging from 0.26% to 1.20%, with the SRSR-(61,2) adduct having mutation frequency of 0.46% (Chary et al., 1995). This result differed from experiments (Wei et al., 1993, 1994) using Chinese hamster V-79 cells, randomly modified with either (+)- or (−)-DE2. The latter results suggested that, at adenines, predominantly A → C mutations occurred at low doses of (+)-DE2, although A → G mutations were observed at low frequency. In contrast, V-79 cells randomly modified with (−)-DE2 yielded fewer mutations and did not exhibit a greater tendency toward mutations at adenine at low dosages, and (−)-DE2 showed less selectivity in its mutagenic profile (Wei et al., 1994). The differences suggested the role of adduct stereochemistry in modulating the mutagenic spectrum. An oligodeoxynucleotide in which a dG mismatch was placed opposite the ^{S,R,S,R}A adduct (Schurter et al., 1995b) yielded a structure similar to that presented here for the SRSR(61,2) adduct. The $^{S,R,S,R}A \cdot G$ mismatch structure modeled a transient intermediate which could lead to A → C transversions (Wei et al., 1991, 1993, 1994). In contrast, structural studies on an ^{R,S,R,S}A adduct arising from (+)-DE2, placed in the corresponding $^{R,S,R,S}A \cdot G$ mismatch context, revealed increased thermal stabilization and an unusual *syn* glycoside torsion angle at ^{R,S,R,S}A (Yeh et al., 1995). One difference between the present $^{S,R,S,R}A \cdot T$ base pair and the $^{S,R,S,R}A \cdot G$ mismatch structures was the presence of a minor conformation in slow exchange with the major intercalated conformation in the mismatch structure (Schurter et al., 1995b). Our NOE data for the $^{S,R,S,R}A \cdot T$ structure show no evidence of minor conformations. The sequence utilized in the studies of the ^{R,S,R,S}A (Yeh et al., 1995) and ^{S,R,S,R}A (Schurter et al., 1995b) adducts opposite dG in the complementary strand differed from the *ras61* oligodeoxynucleotide, in changing the 3′-neighboring base to the site of lesion from adenine to cytosine. Future studies on ^{S,R,S,R}A opposite dG and dC in the *ras61* oligodeoxynucleotide will examine the stabilities and geometries of the mismatched adducted base pairs, in an effort to correlate the structural studies with the mutagenesis results (Wei et al., 1993, 1994; Chary et al., 1995).

Comparison to Replication Studies. Factors likely to contribute to the fate of benzo[*a*]pyrene adducts *in vivo* include repair competence, sequence context (Zarbl et al., 1985; Topal et al., 1986, 1988; Glickman et al., 1987; Randall et al., 1987; Burnouf et al., 1989; Rodriguez & Loechler, 1993; Shibutani & Grollman, 1993; Wilson et al., 1993; Latham & Lloyd, 1994), and the ability of replication complexes to bypass the damage. Primer-extension studies

[4] As noted by Schurter et al. (1995b), chirality at C10 of the adducted benzo[*a*]pyrene did not predict the geometry of benzo[*a*]pyrene guanine N2 adducts in the minor groove.

using HIV-1 reverse transcriptase, Klenow fragment, Sequenase 2.0, T4 polymerase holoenzyme, and human polymerases α and β revealed that when single encounters between the polymerases and the SRSR(61,2) benzo[*a*]-pyrene-adducted *ras61* substrate were permitted, replication was blocked one nucleotide 3′ to the site of lesion on the modified strand (Chary & Lloyd, 1995). Under multiple hit conditions, primer extension was dependent on the identity of the polymerase. The exo^+ polymerases allowed elongation of the primer up to the lesion site. Conversely, the exo^- polymerases allowed full-length extension.

The *in vitro* replication studies (Chary et al., 1995; Chary & Lloyd, 1995) indicated the influence of benzo[*a*]pyrene stereochemistry at C10 upon replication. Hence, it was of interest to compare this structure of the SRSR(61,2) adduct with the (+)-(7*R*,8*S*,9*R*,10*S*)-N^6-[10-(7,8,9,10-tetrahydrobenzo[*a*]pyrenyl)]-2′-deoxyadenosyl adduct [the RSRS(61,2) adduct]. The latter equilibrated between two different conformations with an intermediate rate of exchange on the NMR time scale, which prevented NMR analysis. The corresponding S(61,2) styrene oxide adduct also equilibrated between two different conformations which exchanged at an intermediate rate on the NMR time scale (Feng et al., 1996). However, the sequence isomer S(61,3) styrene oxide adduct, in which the lesion was located one nucleotide downstream, did not exhibit conformational exchange, a result which highlighted the importance of sequence context in characterizing adenine N6 adducts. We speculate that this sequence effect may also be operative for the ^{R,S,R,S}A adduct. Accordingly, future structural studies will be extended to the RSRS(61,3) adduct.

Summary. The SRSR(61,2) (−)-(7*S*,8*R*,9*S*,10*R*)-N^6-[10-(7,8,9,10-tetrahydrobenzo[*a*]pyrenyl)]-2′-deoxyadenosyl adduct formed a quasi-intercalated structure on the 5′-face of the adducted adenine, in which the pyrenyl moiety was inserted into the helix from the major groove. This intercalated structure was similar to that previously observed for the corresponding diastereomer of benzo[*c*]phenanthrene and the (−)-7*R*,8*S*,9*R*,10*R*)-N^6-[10-(7,8,9,10-tetrahydrobenzo[*a*]pyrenyl)]-2′-deoxyadenosyl adduct opposite dT but different from the structure observed for the R(61,2)-α-styrene oxide adduct, which was in the major groove (Feng et al., 1995). Only one conformation was observed, in contrast to the structure of the ^{S,R,S,R}A adduct opposite the incorrect nucleotide dG (Schurter et al., 1995b). The results suggest the importance of stereochemistry at C10 in determining the 5′- or 3′-orientation of the adenine N6 lesion but indicate that the structure of the aromatic moiety plays a role in determining intercalated vs groove binding.

ACKNOWLEDGMENT

Mr. Markus Voehler assisted with NMR spectroscopy and structural refinement. Dr. Parvathi Chary and Professor R. Stephen Lloyd (The University of Texas Medical Branch, Galveston) provided helpful discussions.

SUPPORTING INFORMATION AVAILABLE

Tables S1−S43, which detail the ^{1}H NMR chemical shift assignments and the experimental distances and classes of restraints, and Figure S1, which shows the starting structures used in the MD calculations (17 pages). Ordering information is given on any current masthead page.

REFERENCES

Arnott, S., & Hukins, D. W. L. (1972) *Biochem. Biophys. Res. Commun. 47*, 1504−1509.
Balmain, A., & Brown, K. (1988) *Adv. Cancer Res. 51*, 147−182.
Barbacid, M. (1987) *Annu. Rev. Biochem. 56*, 779−827.
Bax, A., & Davis, D. G. (1985) *J. Magn. Reson. 65*, 355−360.
Bax, A., Sklenar, V., & Clore, G. M. (1987) *J. Am. Chem. Soc. 109*, 6511−6513.
Beland, F. A., & Harvey, R. G. (1976) *J. Chem. Soc., Chem. Commun.*, 84−85.
Bodenhausen, G., Kogler, H., & Ernst, R. R. (1984) *J. Magn. Reson. 58*, 370−388.
Boelens, R., Scheek, R. M., Dijkstra, K., & Kaptein, R. (1985) *J. Magn. Reson. 62*, 378−386.
Borer, P. N. (1975) in *Handbook of biochemistry and molecular biology*, CRC Press, Cleveland, OH.
Borgias, B. A., & James, T. L. (1990) *J. Magn. Reson. 87*, 475−487.
Brooks, B. R., Bruccoleri, R. E., Olafson, B. D., States, D. J., Swaminathan, S., & Karplus, M. (1983) *J. Comput. Chem. 4*, 187−217.
Brunger, A. T. (1992) in *X-PLOR. Version 3.1. A system for X-ray Crystallography and NMR*, Yale University Press, New Haven, CT.
Burnouf, D., Koehl, P., & Fuchs, R. P. P. (1989) *Proc. Natl. Acad. Sci. U.S.A. 86*, 4147−4151.
Cha, R. S., Thilly, W. G., & Zarbl, H. (1994) *Proc. Natl. Acad. Sci. U.S.A. 91*, 3749−3753.
Chary, P., & Lloyd, R. S. (1995) *Nucleic Acids Res. 23*, 1398−1405.
Chary, P., Latham, G. J., Robberson, D. L., Kim, S. J., Han, S., Harris, C. M., Harris, T. M., & Lloyd, R. S. (1995) *J. Biol. Chem. 270*, 4990−5000.
Clore, G. M., Gronenborn, A. M., Carlson, G., & Meyer, E. F. (1986) *J. Mol. Biol. 190*, 259−267.
Cosman, M., De Los Santos, C., Fiala, R., Hingerty, B. E., Singh, S. B., Ibanez, V., Margulis, L. A., Live, D., Geacintov, N. E., Broyde, S., & Patel, D. J. (1992) *Proc. Natl. Acad. Sci. U.S.A. 89*, 1914−1918.
Cosman, M., De Los Santos, C., Fiala, R., Hingerty, B. E., Ibanez, V., Luna, E., Harvey, R., Geacintov, N. E., Broyde, S., & Patel, D. J. (1993a) *Biochemistry 32*, 4145−4155.
Cosman, M., Fiala, R., Hingerty, B. E., Laryea, A., Lee, H., Harvey, R. G., Amin, S., Geacintov, N. E., Broyde, S., & Patel, D. (1993b) *Biochemistry 32*, 2488−2497.
Cosman, M., Fiala, R., Hingerty, B. E., Amin, S., Geacintov, N. E., Broyde, S., & Patel, D. J. (1994a) *Biochemistry 33*, 11507−11517.
Cosman, M., Fiala, R., Hingerty, B. E., Amin, S., Geacintov, N. E., Broyde, S., & Patel, D. J. (1994b) *Biochemistry 33*, 11518−11527.
Cosman, M., Laryea, A., Fiala, R., Hingerty, B. E., Amin, S., Geacintov, N. E., Broyde, S., & Patel, D. J. (1995a) *Biochemistry 34*, 1295−1307.
Cosman, M., Xu, R., Hingerty, B. E., Amin, S., Harvey, R. G., Geacintov, N. E., Broyde, S., & Patel, D. J. (1995b) *Biochemistry 34*, 6247−6260.
De Los Santos, C., Cosman, M., Hingerty, B. E., Ibanez, V., Margulis, L. A., Geacintov, N. E., Broyde, S., & Patel, D. J. (1992) *Biochemistry 31*, 5245−5252.
Feigon, J., Leupin, W., Denny, W. A., & Kearns, D. R. (1983) *Biochemistry 22*, 5943−5951.
Feng, B., & Stone, M. P. (1995) *Chem. Res. Toxicol. 8*, 821−832.
Feng, B., Zhou, L., Passarelli, M., Harris, C. M., Harris, T. M., & Stone, M. P. (1995) *Biochemistry 34*, 14021−14036.
Feng, B., Voehler, M., Zhou, L., Passarelli, M., Harris, C. M., Harris, T. M., & Stone, M. P. (1996) *Biochemistry* (in press).
Fountain, M. A., & Krugh, T. R. (1995) *Biochemistry 34*, 3152−3161.
Glickman, B. W., Horsfall, M. J., Gordon, A. J. E., & Burns, P. A. (1987) *Environ. Health Perspect. 76*, 29−32.
Guengerich, F. P. (1992) *FASEB J. 6*, 745−748.
Hare, D. R., Wemmer, D. E., Chou, S. H., Drobny, G., & Reid, B. R. (1983) *J. Mol. Biol. 171*, 319−336.
Harris, C. M., Zhou, L., Strand, E. A., & Harris, T. M. (1991) *J. Am. Chem. Soc. 113*, 4328−4329.

Harris, T. M., Harris, C. M., Kim, S. J., Kim, H. Y., & Zhou, L. (1994) in *Polycyclic Aromatic Compounds* (Cavalieri, E., & Rogan, E., Eds.) pp 9−16, Harwood Academic Press, Philadelphia, PA.
Havel, T. F., & Wuthrich, K. (1985) *J. Mol. Biol. 182*, 281−294.
Hingerty, B. E., Figueroa, S., Hayden, T. L., & Broyde, S. (1989) *Biopolymers 28*, 1195−1222.
Huberman, E., Sachs, L., Yang, S. K., & Gelboin, H. V. (1976) *Proc. Natl. Acad. Sci. U.S.A. 73*, 607−611.
Jeffrey, A. M., Weinstein, I. B., Jennette, K. W., Grzeskowiak, K., Nakanishi, K., Harvey, R. G., Autrup, H., & Harris, C. (1977) *Nature 269*, 348−350.
Jennette, K. W., Jeffery, A. M., Blobstein, S. H., Beland, F. A., Harvey, R. G., & Weinstein, I. B. (1977) *Biochemistry 16*, 932−938.
Keepers, J. W., & James, T. L. (1984) *J. Magn. Reson. 57*, 404−426.
Kim, S. J., Harris, C. M., Koreeda, M., & Harris, T. M. (1991) *Tetrahedron Lett. 32*, 6073−6076.
Kim, S. J., Stone, M. P., Harris, C. M., & Harris, T. M. (1992) *J. Am. Chem. Soc. 114*, 5480−5481.
King, H. W. S., Osborne, M. R., Beland, F. A., Harvey, R. G., & Brookes, P. (1976) *Proc. Natl. Acad. Sci. U.S.A. 73*, 2679−2681.
Lakshman, M. K., Sayer, S. M., Yugi, H., & Jerina, D. M. (1992) *J. Org. Chem. 57*, 4585−4590.
Latham, G. J., & Lloyd, R. S. (1994) *J. Biol. Chem. 269*, 28527−28530.
Madrid, M., Llinas, E., & Llinas, M. (1991) *J. Magn. Reson. 93*, 329−346.
Mao, B., Xu, J., Li, B., Margulis, L. A., Smirnov, S., Ya, N. Q., Courtney, S. H., & Geacintov, N. E. (1995) *Carcinogenesis 16*, 357−365.
Marion, D., Ikura, M., & Bax, A. (1989) *J. Magn. Reson. 84*, 425−430.
Miller, E. C. (1978) *Cancer Res. 38*, 1479−1496.
Miller, J. A. (1970) *Cancer Res. 30*, 559−576.
Mujeeb, A., Kerwin, S. M., Kenyon, G. L., & James, T. L. (1993) *Biochemistry 32*, 13419−13431.
Nakanishi, K., Kasai, H., Cho, H., Harvey, R. G., Jeffery, A. M., Jennette, K. W., & Weinstein, I. B. (1977) *J. Am. Chem. Soc. 99*, 258−260.
Newbold, R. F., & Brookes, P. (1976) *Nature 261*, 52−54.
Nilsson, L., Clore, G. M., Gronenborn, A. M., Brunger, A. T., & Karplus, M. (1986) *J. Mol. Biol. 188*, 455−475.
Osborne, M. R., Jacobs, S., Harvey, R. G., & Brookes, P. (1981) *Carcinogenesis 2*, 553−558.
Quintanilla, M., Brown, K., Ramsden, M., & Balmain, A. (1986) *Nature 322*, 78−80.
Randall, S. K., Eritja, R., Kaplan, B. E., Petruska, J., & Goodman, M. F. (1987) *J. Biol. Chem. 262*, 6864−6870.
Ravishankar, G., Swaminathan, S., Beveridge, D. L., Lavery, R., & Sklenar, H. (1989) *J. Biomol. Struct. Dyn. 6*, 669−699.
Rodriguez, H., & Loechler, E. L. (1993) *Biochemistry 32*, 1759−1769.
Ryckaert, J.-P., Ciccotti, G., & Berendsen, H. J. C. (1977) *J. Comput. Phys. 23*, 327−341.
Schurter, E. J., Sayer, J. M., Oh-hara, T., Yeh, H. J. C., Yagi, H., Luxon, B. A., Jerina, D. M., & Gorenstein, D. G. (1995a) *Biochemistry 34*, 9009−9020.
Schurter, E. J., Yeh, H. J. C., Sayer, J. M., Lakshman, M. K., Yagi, H., Jerina, D. M., & Gorenstein, D. G. (1995b) *Biochemistry 34*, 1364−1375.
Shibutani, S., & Grollman, A. P. (1993) *J. Biol. Chem. 268*, 11703−11710.
Sims, P., Grover, P. L., Swaisland, A., Pal, K., & Hewer, A. (1974) *Nature 252*, 326−327.
Sklenar, V., Brooks, B. R., Zon, G., & Bax, A. (1987) *FEBS Lett. 216*, 249−252.
Topal, M. D. (1988) *Carcinogenesis 9*, 691−696.
Topal, M. D., Eadie, J. S., & Conrad, M. (1986) *J. Biol. Chem. 261*, 9879−9885.
Wei, S. J., Chang, R. L., Wong, C. Q., Bhachech, N., Cui, X. X., Hennig, E., Yagi, H., Sayer, J. M., Jerina, D. M., Preston, B. D., & Conney, A. H. (1991) *Proc. Natl. Acad. Sci. U.S.A. 88*, 11227−11230.
Wei, S. J., Chang, R. L., Bhachech, N., Cui, X. X., Merkler, K. A., Wong, C. Q., Hennig, E., Yagi, H., Jerina, D. M., & Conney, A. H. (1993) *Cancer Res. 53*, 3294−3301.
Wei, S. J., Chang, R. L., Hennig, E., Cui, X. X., Merkler, K. A., Wong, C. Q., Yagi, H., Jerina, D. M., & Conney, A. H. (1994) *Carcinogenesis 15*, 1729−1735.
Weinstein, I. B., Jeffrey, A. M., Jennette, K. W., & Blobstein, S. H. (1976) *Science 193*, 592−595.
Weisz, K., Shafer, R. H., Egan, W., & James, T. L. (1994) *Biochemistry 33*, 354−366.
Wilson, W. D., Ratmeyer, L., Zhao, M., Strekowski, L., & Boykin, D. (1993) *Biochemistry 32*, 4098−4104.
Wolfe, A., Shimer, G. H., Jr., & Meehan, T. (1987) *Biochemistry 26*, 6392−6396.
Wuthrich, K. (1986) in *NMR of proteins and nucleic acids*, John Wiley & Sons, New York.
Yagi, H., Hernandez, O., & Jerina, D. M. (1975) *J. Am. Chem. Soc. 97*, 6681−6683.
Yeh, H. J. C., Sayer, J. M., Liu, X., Altieri, A. S., Byrd, R. A., Lakshman, M. K., Yagi, H., Schurter, E. J., Gorenstein, D. G., & Jerina, D. M. (1995) *Biochemistry 34*, 13570−13581.
Zarbl, H., Sukumar, S., Arthuyr, A. V., Martin-Zanca, D., & Barbacid, M. (1985) *Nature 315*, 382−385.
Zegar, I. S., Setayesh, F. R., DeCorte, B. L., Harris, C. M., Harris, T. M., & Stone, M. P. (1996) *Biochemistry 35*, 4334−4348.

BI9524732